JOURNAL OF GEOPHYSICAL RESEARCH, VOL. 111, A11S17, doi:10.1029/2006JA011627, 2006

Magnetospheric current systems during stormtime sawtooth events

T. I. Pulkkinen,[1,2] N. Y. Ganushkina,[2] E. I. Tanskanen,[2] M. Kubyshkina,[3] G. D. Reeves,[1] M. F. Thomsen,[1] C. T. Russell,[4] H. J. Singer,[5] J. A. Slavin,[6] and J. Gjerloev[7]

Received 23 January 2006; revised 19 April 2006; accepted 22 May 2006; published 28 September 2006.

[1] The sawtooth event period embedded in a storm interval on 2001-10-22 is analyzed using magnetic field modeling techniques. The model current systems show that sawtooth injections are associated with strong stretching of both the nightside and dusk-sector magnetic field prior to the injection and a partial disruption of that current at the time of the injection. The currents are strongest near geosynchronous distance and in the premidnight sector. The strong dusk-sector field stretching produces very fast proton drift speeds, which can explain the near-simultaneous occurrence of the injections over a wide local time sector. Comparison of sawtooth periods with nonstorm substorms indicates that the tail field behavior resembles that of nonstorm substorms, but that the consequences of the stretching/dipolarization cycle are different from nonstorm times. As the drifting protons during sawtooth events are mostly on open drift paths, the symmetric ring current is only slightly affected, while large variations are seen in the asymmetric ring current. The three-spacecraft magnetic field measurements together with the *Dst* index were sufficient to constrain the magnetic field model to give a reasonably accurate global magnetic field representation, as confirmed by an independent test using measurements not used in the fitting. Thus we conclude that the empirical modeling methods can be quite reliable in predicting the large-scale fields when suitable observations are available.

Citation: Pulkkinen, T. I., N. Y. Ganushkina, E. I. Tanskanen, M. Kubyshkina, G. D. Reeves, M. F. Thomsen, C. T. Russell, H. J. Singer, J. A. Slavin, and J. Gjerloev (2006), Magnetospheric current systems during stormtime sawtooth events, *J. Geophys. Res.*, *111*, A11S17, doi:10.1029/2006JA011627.

1. Introduction

[2] The inner magnetosphere is a complex region with highly varying electromagnetic fields and multiple plasma populations present at all times. Yet it is the region where accurate forecasts of the space environment are most needed, as it hosts the majority of the Earth-orbiting spacecraft in the very hostile particle environment. As the complexity of the fields and particle distribution functions makes accurate representation of the plasma environment challenging, key questions both for scientific research and space weather forecasts center around the models that we have available today are: To what extent can they provide a predictive capability? What is the level of model sophistication needed for sufficient accuracy? What are the best dynamic equations to accurately describe the inner magnetospheric physics?

[3] The inner magnetospheric dynamics is at its most variable during magnetic storms, when the magnetic and electric fields are highly disturbed, and the energetic ion and electron fluxes increase by orders of magnitude. The magnetic activity during storms is much more complex than under nonstorm conditions and has been under intense study recently. Depending on data sets and analysis methods used, stormtime substorms have been judged to be qualitatively different from nonstorm ones, while some researchers have argued that even if stormtime substorms may have features distinct from the nonstorm ones, most of them can be categorized as substorms [*Henderson*, 2004; *Pulkkinen et al.*, 2005].

[4] To avoid semantic problems associated with the definition of what is and what is not a substorm, in this paper we call rapid enhancements of the westward electrojet seen as significant decreases in the ground magnetometer X componenets ''activations'' rather than ''substorms.'' This allows for a variety of associated tail signatures, some of which may be analogous to substorms while others may not.

[5] Sawtooth events are a particular set of magnetospheric activations, which are most often observed during storm periods. At geostationary orbit, they are characterized by quasiperiodic injections expanding over the terminators within a few minutes of the injection. Furthermore, they are

[1]Los Alamos National Laboratory, Los Alamos, New Mexico, USA.
[2]Finnish Meteorological Institute, Helsinki, Finland.
[3]St. Petersburg State University, St. Petersburg, Russia.
[4]Institute for Geophysics and Planetary Physics, University of California, Los Angeles, Los Angeles, California, USA.
[5]Space Environment Center, Boulder, Colorado, USA.
[6]NASA Goddard Space Flight Center, Greenbelt, Maryland, USA.
[7]Johns Hopkins University Applied Physics Laboratory, Laurel, Maryland, USA.

0148-0227/06/2006JA011627$09.00

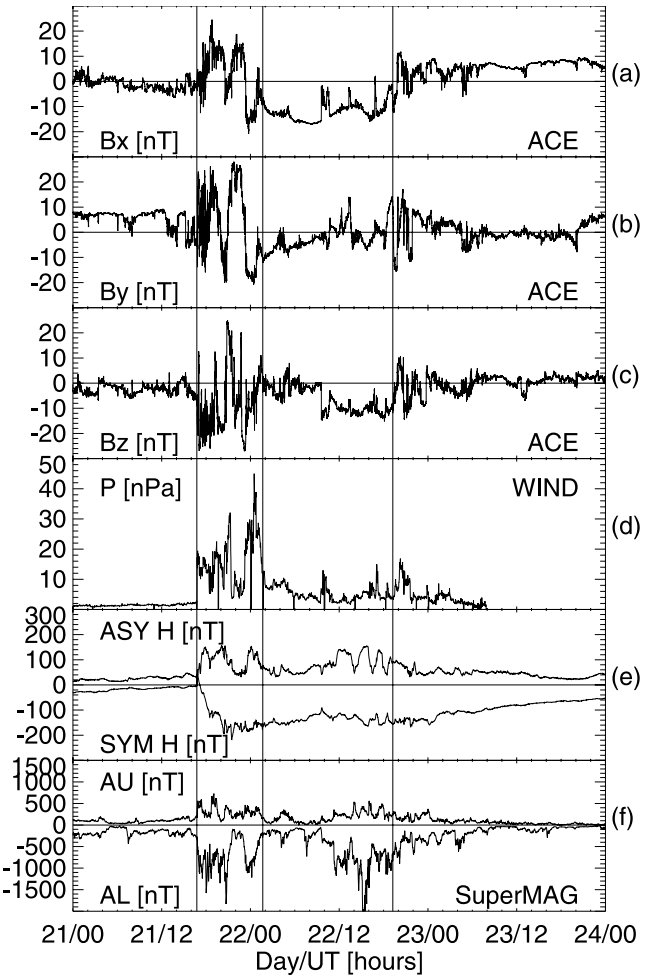

Figure 1. 2001-10-21-22: Solar wind and IMF observations. Magnetic field components (a) B_X, (b) B_Y, and (c) B_Z from ACE (all in GSM coordinates, data are lagged by 36.7 min to account for the traveltime from the spacecraft to the average magnetopause position); (d) Solar wind dynamic pressure from WIND (lagged 4.5 min); (e) ASY-H and SYM-H indices; (f) AU and AL indices created using data from 80 stations from the SuperMAG network. The vertical lines show the storm onset, and the magnetic cloud begin and end times.

characterized by an extremely stretched magnetic field at synchronous orbit [*Reeves et al.*, 2004; *Henderson*, 2004; *Huang et al.*, 2005]. While in many respects these activations resemble nonstorm substorms [*Lui et al.*, 2004], their wide longitudinal extent, rapid propagation speed, and periodicity of about 2.5 hours raise important questions of what drives these global-scale magnetospheric oscillations, and what magnetospheric and ionospheric current systems support such development.

[6] Empirical models of the electromagnetic fields provide a means to examine the magnetospheric current systems, and combined with drift calculations, a possibility to study the acceleration of both ring current ions and outer van Allen belt electrons. The most widely used field models developed by *Tsyganenko* [1989; 1995] provide a good representation of the average magnetospheric configuration but cannot account for the shorter timescale variations of the magnetic field during substorms or the large field changes during intense storms. Statistical models designed specifically to represent the storm-time inner magnetosphere have also been developed by parametrizing the magnetospheric field configuration dependence on the state of the external solar wind and interplanetary magnetic field (IMF) [*Tsyganenko*, 2002a, 2002b]. While these models are good for following the large-scale evolution of the field, again they cannot reproduce the fine structure of the stormtime substorms or other activations.

[7] Attempting to gain an accurate representation of the magnetospheric configuration during specific events, event-oriented methods use observations to determine the current systems at any given time [*Ganushkina et al.*, 2002, 2004]. Such models have allowed us to study the evolution of the magnetospheric current systems during storms of varying intensity. Specifically, we have addressed the long-standing issue of the relative contributions of the tail and ring currents during storms [*Skoug et al.*, 2003; *Ganushkina et al.*, 2004; *Kalegaev et al.*, 2005]: It was demonstrated that during moderate magnetic storms the tail current intensification is a major contributor to the Dst-enhancement, but that during intense storms it is the ring current proper that accounts for the large magnetic disturbances seen in mid-latitude magnetograms.

[8] In this paper we examine in detail the magnetotail activity during a sawtooth event that was observed during the Earth passage of the trailing edge of a magnetic cloud on 2001-10-22. Interestingly, the energy input and output to and from the magnetosphere were in balance such that the Dst index remained almost constant at the level of near −150 nT over a 24-hour period [*Pulkkinen et al.*, 2005]. The sawtooth injections were observed toward the end of this period, associated with relatively strong solar wind driving and intense high-latitude magnetic activity. Using this event as a representative example, we will discuss the stormtime magnetic activations, energy circulation and its drivers during storms, the relationship between sawtooth events and substorms, and the interaction between the magnetotail and the ring current. With these results, we address the requirements for models to adequately represent the complexity of the inner magnetosphere.

2. Observations

2.1. Storm Overview

[9] The storm initiated when the sheath region of an interplanetary magnetic cloud reached the magnetosphere at 1645 UT on 2001-10-22. The shock was driven by a velocity jump from about 400 to 600 km/s. In the sheath region, the IMF B_Z was variable but mostly negative. Following the sheath encounter, the magnetosphere was embedded within the cloud proper (0140–1915 UT on 22 October), which had a large negative B_X and slowly rotating B_Y and B_Z. The IMF B_Z was close to zero at the leading edge of the cloud, while it was negative during the latter part of the cloud. Magnetic field measurements from MAG instrument onboard the ACE spacecraft [*Smith et al.*, 1998] in the interplanetary space are shown in the top three panels of Figure 1.

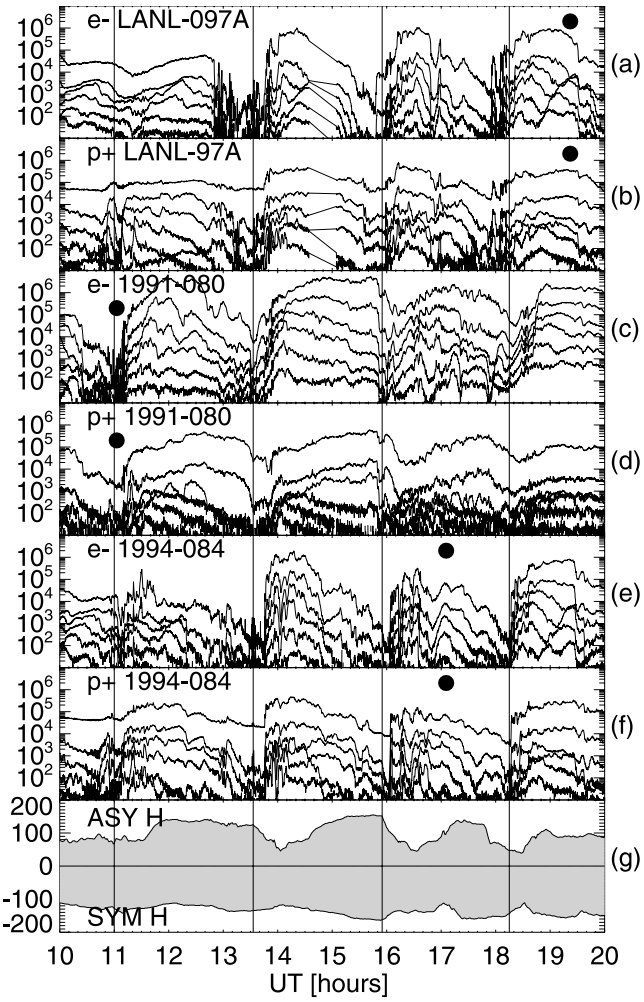

Figure 2. 2001-10-22: Differential fluxes (a) electrons from LANL-097A, (b) protons from LANL-097A, (c) electrons from 1991-080, (d) protons from 1991-080, (e) electrons from 1994-084, and (f) protons from 1994-084 spacecraft. Local midnight is indicated by the black dot for each spacecraft. The fluxes are given in units of 1/(cm^2 sr s keV). Energy channels for electrons are 50–75, 75–105, 105–150, 150–225, 225–315, and 315–500 keV and for protons 50–75, 75–113, 113–170, 170–250, 250–400, 400–670 keV. (g) ASY-H and SYM-H indices in nT.

[10] The solar wind dynamic pressure was large and highly variable during the sheath encounter ranging from a few nPa to above 40 nPa during the encounter, while it was smoother but remained around 10 nPa during the following magnetic cloud. Solar wind pressure observations from the SWE experiment onboard the Wind spacecraft [*Ogilvie et al.*, 1995] upstream of the magnetosphere are shown also in Figure 1d. The largest pressure enhancements together with the negative B_Z were strong enough to push the magnetopause inside geosynchronous orbit [*Pulkkinen et al.*, 2005].

[11] The Wind spacecraft was at (43.3, −7.5, 6.5) R_E at the shock onset and moved to (22.3, 7.0, −0.1) R_E by the end of 22 October. The ACE satellite at the L1 point moved from (220.9, 4.7, 26.2) R_E to (220.7, 11.1, 25.3) R_E (GSM coordinates) during the same time period. The average travel times from the satellite position to the magnetopause were 4.5 min for Wind and 36.7 min for ACE, assuming only motion in the X direction. All solar wind and IMF data are shown with these time shifts included.

[12] The two bottom panels of Figure 1 show the magnetic indices describing midlatitude and high-latitude magnetic activity. The SYM-H index varied between −130 and −160 nT and was relatively constant over an extended time period from the main phase maximum through the end of the magnetic cloud passage. The ASY-H index was highly variable and reached values above 150 nT. The standard interpretation of these observations is that while the symmetric part of the ring current remained relatively constant, the asymmetric ring current was very strong and highly variable during the storm [*Iyemori and Rao*, 1996].

[13] The auroral activity was concentrated on two periods, first during the cloud sheath encounter and later during the trailing edge of the cloud when the IMF was again strongly negative. Both periods were characterized by strong and almost continuous AL activity reaching well below −1500 nT. The AU and AL indices shown in Figure 1f were created using 80 magnetograms from the SuperMAG network.

2.2. Sawtooth Injection Observations

[14] Figure 2 shows the geosynchronous energetic electron and proton measurements from the SOPA instruments onboard three LANL spacecraft [*Belian et al.*, 1992]. The sawtooth injections can be seen as four distinct flux enhancements in both electrons and protons. The filled circle in each panel denotes the time of local midnight of the satellites. It is obvious that the injections are near-simultaneous both in electrons and in protons, and over a wide range of local times. The SYM-H and ASY-H indices are repeated in the bottom panels for reference. The vertical lines show the injection onset times for all four sawteeth. These times should be considered only as reference times to help reading the figures and are not meant to imply exact knowledge of the actual onset times of the injection processes.

[15] Figure 3 shows magnetic field measurements both from ground and space. The vertical lines mark the times of the sawtooth injection onsets. The top panel shows the midlatitude SYM-H and ASY-H indices. The injections do not cause marked signatures in the SYM-H index other than a slight reduction following each sawtooth. On the other hand, the ASY-H index generally responds to the injections by an initial decrease followed by delayed increase. The AL-index shows enhanced auroral-latitude activity throughout the period. The first two sawteeth show an associated AL intensification, which, however, is delayed with respect to the geostationary orbit injection onset. The third and fourth injections show simultaneous enhancement, but not very pronounced intensity increase.

[16] The three bottom panels depict the magnetic field variations in the inner magnetosphere. Magnetic field measurements are shown from GOES-8 in the morning sector and GOES-10, which passed through midnight slightly before the first sawtooth injection (see *Singer et al.* [1996] for instrument details). Polar was in the night sector plasma sheet at about 8 R_E distance and 22 MLT.

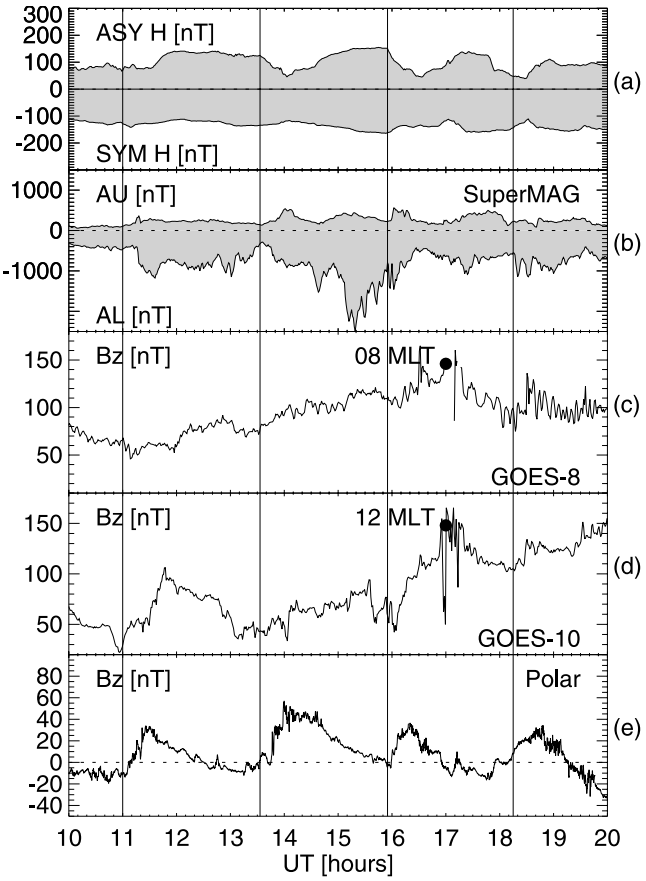

Figure 3. 2001-10-22: (a) ASY-H and SYM-H indices; (b) AU and AL indices created using data from 80 stations from the SuperMAG network; Magnetic field B_Z components from (c) GOES-8, (d) GOES-10, and (e) Polar (all in GSM coordinates).

Polar magnetic field measurements [*Russell et al.*, 1995] clearly show strong dipolarizations of the magnetic field during each of the sawteeth. The signature is also clear for the first and third sawtooth at GOES-10. The dipolarizations were not as clear in the geostationary orbit magnetic field data away from the midnight sector, but still a moderate field change was visible associated with every sawtooth injection.

[17] The ring current behavior is further analyzed using available northern hemisphere midlatitude ground magnetograms. The top panel of Figure 4 plots the *H*-disturbance color-coded in a UT-MLT diagram, which shows the magnetic disturbance level for all local times as a function of time. The baseline (zero disturbance) was selected to be before the sawtooth event at 1000 UT. In the plot, red colors denote negative *H*-bay while blue colors denote positive *H*-disturbance. It is clear that the ring current was increasingly asymmetric with negative disturbances intensifying in the evening sector.

[18] The bottom panel of Figure 4 shows the auroral latitude magnetic activity in similar format, i.e., color-coded in a UT-MLT diagram. Instead of showing the individual stations at varying magnetic latitudes, the SuperMAG database was divided into six local time sectors to provide limited local time sector indices which are then color-coded in the figure. Comparing the activation intensities clearly shows that the strongest auroral-latitude magnetic activity was concentrated in the morning sector instead of the more typical evening-sector dominance during substorm activity (with the caveat that the evening-sector data coverage was somewhat more limited than that in the morning sector).

3. Event-Oriented Magnetic Field Model

[19] In order to gain understanding of the magnetotail behavior during the sawtooth event, we employ the methods developed by *Ganushkina et al.* [2002, 2004] to model the inner magnetosphere current systems. The basic approach is to begin with the statistical field description given by the T89 model for Kp = 4 [*Tsyganenko*, 1989], modify the existing current systems, and add stormtime current components to the model so that a best fit is obtained with all available high-altitude magnetic field measurements as well as the ground-based Dst index. While newer versions of the empirical models have appeared since T89 [e.g.,

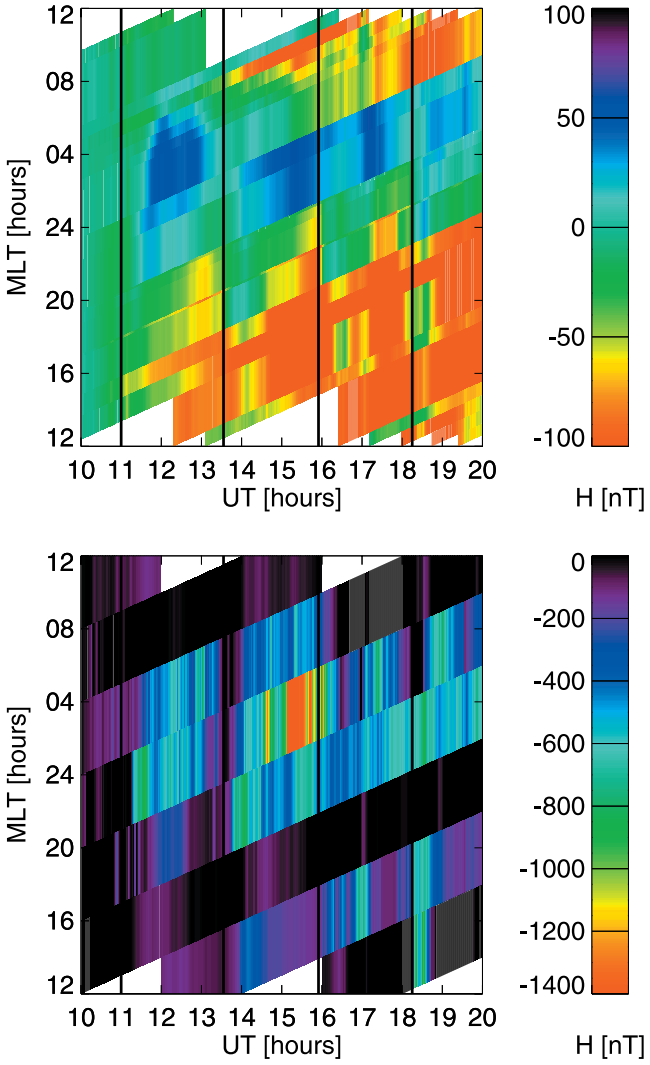

Figure 4. 2001-10-22: UT-MLT plot created using (top) midlatitude and (bottom) auroral latitude magnetograms. The level of magnetic disturbance (in nT) is shown color-coded.

Tsyganenko, 1995, 2002a, 2002b], the T89 was selected as the starting point because it has relative simple description of the magnetospheric current systems and because it is numerically very fast compared to the newer models.

3.1. Ring Current

[20] The ring current module in the T89 model is replaced by two symmetric currents, one flowing eastward closer to the Earth and one flowing westward farther from the Earth. This is done to get a more accurate representation of the field changes associated with the enhancing torus-like ring current. The symmetric ring current intensity J^{SYM} as a function of radial distance in the equatorial plane R_{EQ} and the relative intensity of the magnetic field B/B_0 is given by

$$J\left(\mathbf{R},\frac{B}{B_0}\right)^{SYM}=\sum J_{0,i}\exp\left(-\frac{\left(R_{EQ}-R_{0,i}\right)^2}{2\sigma^2_{R_{EQ}}}\right)\left(\frac{B}{B_0}\right)^{-A/2} \quad (1)$$

where the index i sums over eastward and westward ring currents, B_0 is the magnetic field at the equator, $J_{0,i}$ is the maximum current intensity, $R_{0,i}$ the location of the maximum of the current density, σ is the current distribution width (same for both eastward and westward currents), and A is the anisotropy index determining how concentrated the current is close to the equatorial plane [*Ganushkina et al.*, 2002, 2004].

[21] Similarly, the asymmetric partial ring current J^{PART} is modeled by a function similar to the symmetric ring current but with an added asymmetry factor given by $(1 - \cos(\phi - \delta))$, where ϕ is the azimuth angle and δ is the duskward shift angle giving the azimuthal location of the current maximum. The asymmetry factor gives rise to field-aligned currents in the region 2 sense; these currents are evaluated numerically from the divergence of the asymmetric ring current.

[22] With this formulation, the ring current module includes eight free parameters: the average distances of the current systems ($R_{0,EAST}$, $R_{0,WEST}$, $R_{0,PART}$), maximum current densities ($J_{0,EAST}$, $J_{0,WEST}$, $J_{0,PART}$), current distribution width (σ), and anisotropy index (A). As the duskward shift δ of the partial ring current is known to depend on the level of magnetic activity, it is evaluated from the Dst index as

$$\delta=\frac{\pi}{2}\tanh\left(\frac{|Dst|}{Dst_0}\right) \quad (2)$$

where the reference level is chosen to be Dst_0 = 40 nT [*Tsyganenko*, 2002b].

3.2. Magnetotail Current

[23] The magnetotail current intensity is known to vary strongly depending on the level of solar wind driving: during periods of southward IMF the tail current intensifies and moves earthward. Furthermore, a thin current sheet is often formed near the inner edge of the plasma sheet. That current is often concentrated in a layer that has a half-thickness of the order of the ion Larmor radius, and tailward extent from near-geosynchronous region to about 20 R_E [e.g., *Pulkkinen et al.*, 1992].

[24] We account for the tail current intensification by modifying the T89 tail current intensity by a factor (1 + *ATS*), where *ATS* is a constant determining the increase (positive values) or decrease (negative values) from the baseline T89 model.

[25] In addition to modifying the intensity of the entire tail current, we add a new thin current sheet near the inner edge of the tail current sheet. The new tail current sheet is formulated using vector potentials to ensure that the magnetic field remains divergenceless. The vector potentials are of the form

$$A_i^T=\frac{A_{NTC}W_i\left(X,Y,X_{i,NTC}\right)}{S_T+a_T+\xi_T}\left(C_1+\frac{C_2}{S_T}\right)$$

where i runs from 1 to 2, A_{NTC} gives the intensity of the new current sheet, S_T is a function characterizing the warping of the current sheet, ξ is a function characterizing the distance from the current sheet center, and C_1 and C_2 are constants defining the profile of the current. The cross-tail width functions W are defined by the earthward and tailward edge locations of the current sheet ($X_{1,NTC}$ and $X_{2,NTC}$) and current sheet thickness. For details of the formulation, we refer to *Tsyganenko* [1989] and *Ganushkina et al.* [2002].

[26] The difference of these two vector potentials $A = A_1^T - A_2^T$ gives a thin current sheet with current density given by $\mu_0\mathbf{J} = \nabla \times (\nabla \times \mathbf{A})$ between the limits $X_{1,NTC}$ and $X_{2,NTC}$, and zero current intensity elsewhere. The magnetic field components from this current are then given by $\mathbf{B} = \nabla \times \mathbf{A}$.

[27] The tail current formulation includes five free parameters: Current intensities *ATS* and A_{NTC}, earthward and tailward edge locations of the new thin current sheet $X_{1,NTC}$ and $X_{2,NTC}$, and half-thickness of the thin current sheet D_0.

3.3. Magnetopause Current

[28] As the T89 model does not include an explicit magnetopause and its electric current formulation, modification of the model currents is not as straight forward as in the case of the intramagnetospheric currents. However, it is clear that the magnetopause position and current intensity are strongly controlled by the solar wind pressure [e.g., *Shue et al.*, 1998]. We thus scale the T89 magnetopause field components by a time-varying constant AMP = $\sqrt{P_{SW}/2\text{nPa}}$, where 2 nPa is taken to represent quiet time average solar wind pressure and is used as a normalization constant only. In addition to scaling the dayside Chapman-Ferraro field, it is also necessary to scale the characteristic size of the magnetotail. We scale the tail radius to match that given by *Shue et al.* [1998]. The magnetopause field and the magnetotail radius are then defined by the observed solar wind and IMF parameters in the form

$$\begin{aligned} B_{CF}&=\left(\frac{P_{SW}}{2\,\text{nPa}}\right)^{\frac{1}{2}}B_{CF_{T89}}\\ R_T&=\left(\frac{Z_{T,Shue}}{Z_{T,T89}}\right)R_{T,T89}\end{aligned} \quad (3)$$

where R_T = 30 R_E is the T89 tail radius value for Kp = 4. The magnetopause position Z-coordinates are evaluated

Table 1. Summary of Model Parameters[a]

Current	Parameter	Unit	Fixed	Free	Data
Eastward RC	$R_{0,EAST}$	R_E	2.0		
	$J_{0,EAST}$	nA/m^2	1.5		
Westward RC	$R_{0,WEST}$	R_E		2.5–4.5	
	$J_{0,WEST}$	nA/m^2		1.5–15.0	
Partial RC	$R_{0,PART}$	R_E		5.0–6.5	
	$J_{0,PART}$	nA/m^2		0.5–7.0	
	σ		0.8		
	A		1.0		
	δ				Dst
Tail current	ATS			−0.5–2.0	
	A_{NTC}			0.1–2.4	
	$X_{1,NTC}$	R_E	−2.0		
	$X_{2,NTC}$	R_E	−10.0		
	D_0	R_E	0.2		
MP currents	AMP				P_{SW}
	R_T				P_{SW}, IMF

[a]Left column indicates current system, next the parameter and its physical unit (if any). The three following columns indicate (Fixed) use of fixed value for the parameter, (Free) range of values used in the fitting procedure, and (Data) data used to derive the parameter value.

from the *Shue et al.* [1998] model ($Z_{T,Shue}$) and T89 model ($Z_{T,T89}$) at $X = -20\ R_E$ and $Y = 0$.

[29] The magnetopause current modeling involves only two parameters (AMP and R_T), both of which are directly determined from solar wind and IMF observations.

3.4. Sawtooth Event Model

[30] Using the formulation above and magnetic field measurements from GOES-8, GOES-10, Polar, and the Dst index, the model parameters were evaluated during 1000–2000 UT to give a best fit to the observed field values. As the number of measurement points in the magnetosphere is limited, it is not possible to determine all parameters by the fitting procedure. Table 1 collects the model parameters and indicates parameters that were used with fixed values (not changed by fitting procedure), parameters determined by the Dst index, solar wind pressure, and IMF B_Z (not changed by fitting procedure but variable in time), and the range of allowed values for the six free parameters during the fitting procedure. The best fit was determined by minimizing the least squares error between the model and observed field components in space and on ground. Each time step was fitted individually with linear least squares fitting with no predetermined correlation between neighboring time steps.

[31] Figure 5 shows the results of the fitting procedure during the sawtooth event on 22 October, 1000–2000 UT. Shown are magnetic field B_X (top row), B_Y (middle row), and B_Z (bottom row) components for GOES-8 (left column), GOES-10 (middle column), and Polar (right column) spacecraft. All field values are shown with the dipole field subtracted. Measurements are shown with thin lines and the event-oriented magnetic field model with thick lines. All these measurements were also used in the fitting procedure.

[32] On average, the model predicts the magnetospheric field variations quite well during the course of the storm (mean error was 22 nT). The advantage of the event-oriented model over statistical models such as, for example, the T01s model [*Tsyganenko*, 2002a, 2002b] is that it captures the essential features of the magnetic field stretching and dipolarization seen especially well in the Polar data. The statistical models are specified by solar wind and IMF parameters and the Dst index, which alone cannot define growth phase and onset timings, and typically give weaker stretching and no dipolarizations.

[33] In order to carry out a test of the model performance using independent data, Figure 6 compares field inclination measurements from the MPA-instrument onboard three LANL spacecraft 1991-080, 1994-084, and LANL-97A [*Bame et al.*, 1993]. The field inclinations were inferred from the pitch angle distribution symmetry properties for electrons in the energy range 0.03–40 keV. In case the ion distribution showed stronger anisotropy, the ion data in the energy range 0.1–40 keV were used for the anisotropy determination [*Thomsen et al.*, 1996]. While there are discrepancies, overall the agreement is reasonably good. Spacecraft 1991-080 was near midnight during the first injection, while the same is true for s/c 1994-084 for the third sawtooth. In both cases, the model slightly overpredicts the amount of field stretching in the midnight sector. On the other hand, s/c 1991-080 gives good agreement in the postmidnight sector, and LANL-97A a reasonable fit in the postdusk sector after the second sawtooth. The main difference is that the dipolarizations in the model are not as strong as those observed at geostationary orbit. This is most likely due to the fact that the model lacks the field-aligned currents that can significantly contribute to the field inclination within the current wedge, where both the downward and upward currents act as to increase the field inclination (further dipolarize the field). This is not as much of a problem further out, where the field-aligned currents spread over a wider region of space.

[34] The relatively good agreement in all local time sectors leads us to believe that the magnetic field model captures the essential features of the magnetotail magnetic field variations during the sawtooth events, including the strongly asymmetric conditions both in the noon-midnight and dawn-dusk meridian planes. Further assurance of the model performance is given by the fact that the time series of the various parameters shows a rather smooth behavior even though each time step was fitted individually, as will be discussed in the next section.

4. Analysis of Model Results

[35] Following detailed analyses of sawtooth events, the community is currently debating whether they form a special class of events or are simply storm-time realizations of substorm activity. It is meaningful to categorize these as distinct types of activations only if they are associated with physical processes that are markedly different from those of nonstorm substorms or if they always occur under specific solar wind and/or magnetospheric conditions that can be distinguished from typical substorm conditions.

[36] There were in total five Los Alamos spacecraft measuring the geostationary orbit energetic particle environment, although s/c 1990-095 had data gaps. Thus, good coverage was available during the entire period. While the injections were not completely simultaneous from satellite to satellite, all four injections were seen at all five (or four) spacecraft. The proton injections were first seen in the morning sector, while the electron injections were first observed in the nightside magnetotail (see Figure 2).

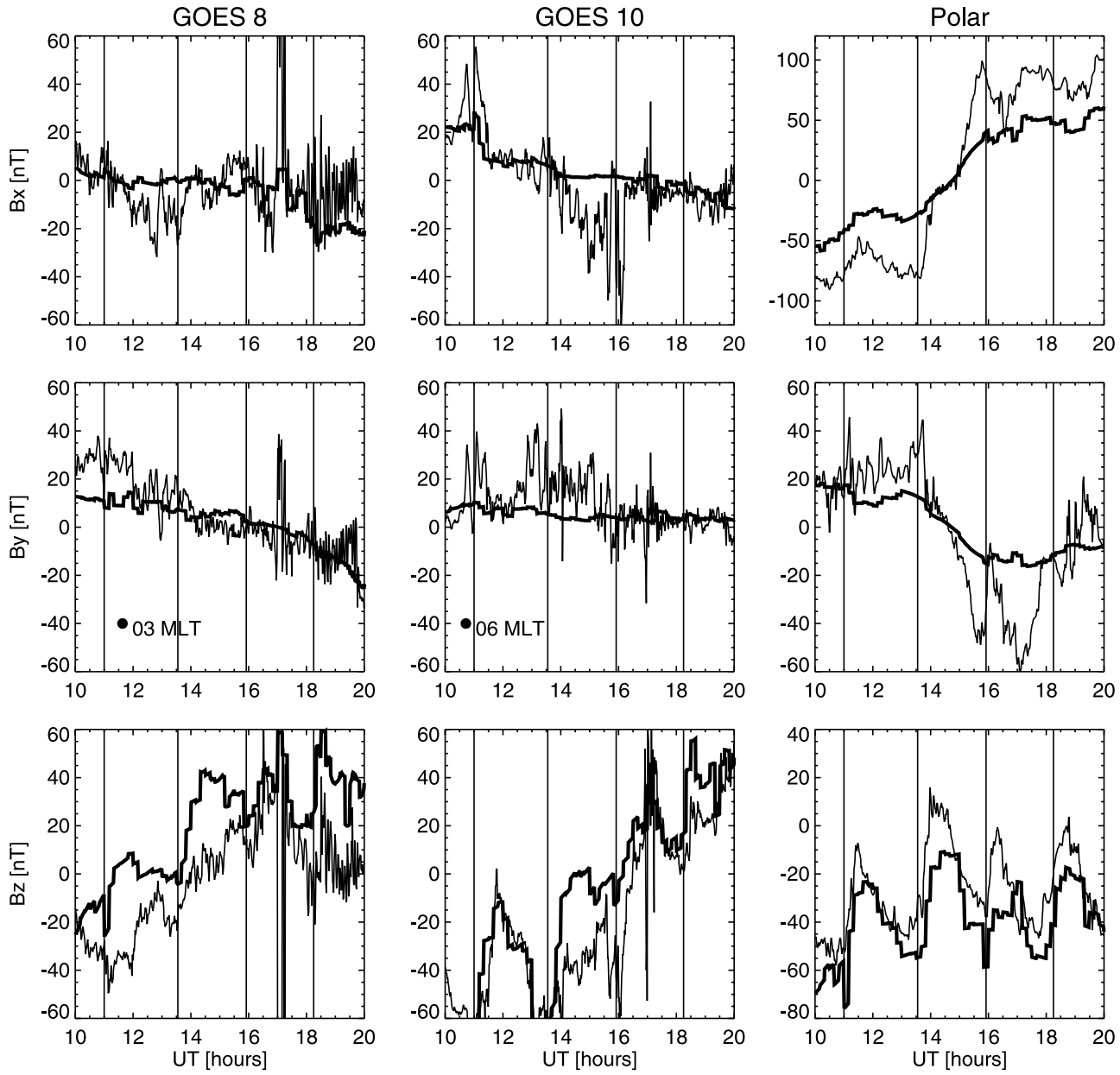

Figure 5. 2001-10-22: Magnetic field model results for GOES-8, GOES-10, and Polar. Panels from top to bottom show B_X, B_Y, and B_Z components of the field with the internal field subtracted (all in GSM coordinates). Observations are shown with thin lines, and the event-oriented field model developed here is shown with thick lines. The solid dots in the B_Y panel shows the times when GOES-8 and GOES-10 were at 0300 and 0600 MLT, respectively.

[37] The magnetic field observations from Polar show that the field dipolarizations were observed promptly during each sawtooth. GOES-10 showed a clear dipolarization at the first and third sawtooth, and somewhat less clear signatures during the second and fourth. GOES-8 showed also field enhancements during the first, third and fourth sawtooth events, and less clear signature during the second.

[38] The field inclination inferred from the MPA data show clear signs of the dipolarizations for all sawteeth in the dusk, midnight, and dawn sectors. The only dipolarization not observed was the first sawtooth at LANL-97A, which at that time was located near 15 MLT. Taken together, each of the four sawteeth extended at least from terminator to terminator within only a few minutes from the onset near the night sector.

[39] Figure 7 shows the model parameters derived from the fitting procedure. The model results are shown with the solid dots. The top panel shows the measured and model-predicted SYM-H indices, which overlap perfectly. The SYM-H index was used in the fitting procedure, and this agreement demonstrates that it is possible to find a magnetospheric current configuration which reproduces the ground magnetic index variations to high degree of accuracy.

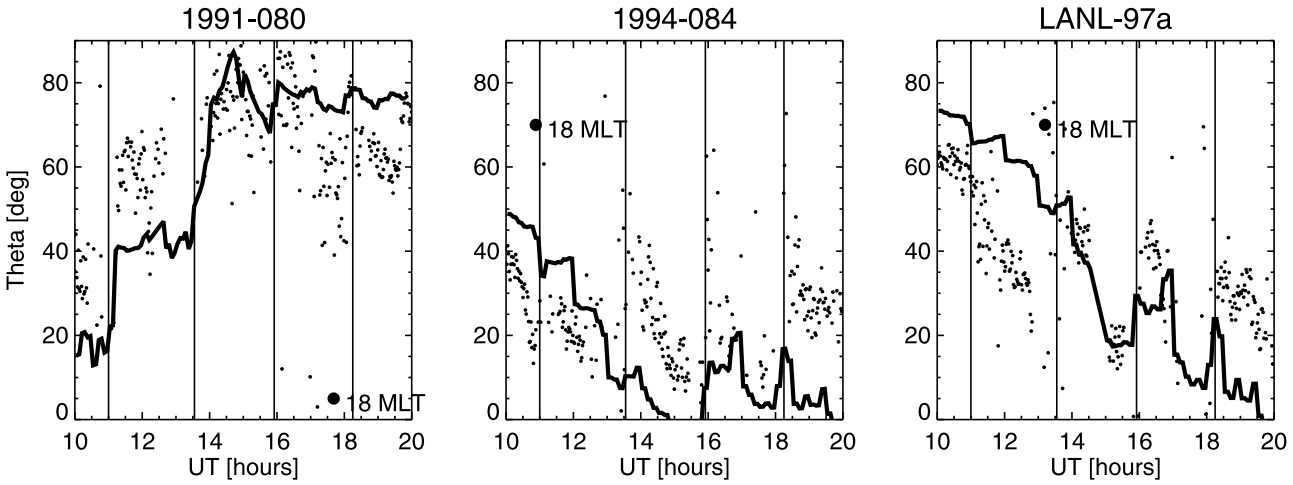

Figure 6. Magnetic field model results compared with field inclination measurements from the MPA instrument onboard LANL geostationary satellites. The polar angle ($\theta = \tan^{-1}(B_Z/\sqrt{B_X^2 + B_Y^2})$ is shown in GSM coordinates with data shown with solid dots and empirical model results with thick solid lines. The solid dots show the times when the s/c were at 18 MLT.

[40] Figure 7b shows the intensity of the symmetric part of the ring current. It shows relatively low degree of variability (except 1300–1400 UT), consistent with the almost constant value of the SYM-H index. Even the slightly decreasing trend in the SYM-H index is reflected as an increase in the total ring current toward the end of the modeling period.

[41] Figures 7c and 7d show the asymmetric index ASY-H and the partial ring current in the model. The partial ring current is much more variable than its symmetric counterpart; it shows a rapid decrease associated with three first sawtooth injections, but a rather curious increase at the time of the fourth injection. The ASY-H index behavior is qualitatively quite similar to the asymmetric ring current, even though the ASY-H index was not used in the fitting procedure. Thus, it seems that both the model and ground magnetic observations indicate the existence of highly variable and strong asymmetric ring current component in the dusk sector magnetotail.

[42] Figures 7e and 7f show the magnetic field measurements from Polar, the model reproduction of the field at that location and the total tail current in the model. Each of the dipolarizations in the magnetotail are associated with a decrease in the tail current. After the decrease, the tail current starts to build up until the next dipolarization follows in about 2 hours' time. This is qualitatively consistent with the standard view of substorm-associated buildup and disruption of the inner magnetosphere tail current. Note that the asymmetric part of the ring current behaves similarly with the tail current, decreasing at the time of the injections and increasing during the periods between the injections. This indicates that the partial ring current is associated with the energy loading and thin current sheet formation processes near the inner edge of the magnetotail [*Pulkkinen et al.*, 1992]. However, the SYM-H index (and the model symmetric ring current) were relatively unchanged during the current disruption and injection events.

[43] The model results presented in Figure 7 describe each of the model current systems individually. However, the current systems overlap, and it is impossible for the model to know which current system creates which part of the variation at the measurement points if the measurements do not cover a substantial portion of local times and radial distances. Therefore the distribution of the model currents to "symmetric ring current," "tail current," and "partial ring current" is somewhat ambiguous. In the following, the currents are separated only based on their location in the magnetosphere.

[44] The top panel of Figure 8 shows the total current inside geostationary orbit (in units of MA) at four local times, midnight (black), noon (red), dusk (blue), and dawn (green). These values were obtained by integrating the current density from $R = 2\ R_E$ to $R = 6.6\ R_E$ and over the entire current sheet thickness. The bottom panels show the integrated current ($\int j_\phi\ dz$, in units of nA/m) as functions of time and X (middle panel) or Y (bottom panel). Hence the middle panel gives the current flowing through the noon-midnight meridian plane, while the bottom panel gives the current through the dawn-dusk meridian plane. The sawtooth injection times are marked with black or white vertical lines.

[45] The middle panel shows that each of the sawtooth injections is preceded by strong enhancement of the tail currents between geosynchronous orbit and about 10 R_E. The first, second, and fourth injections also correspond to times of the tail current disruption. During the third onset the current weakens in the inner magnetosphere around geostationary distance, but the tail current reduces only slightly and remains relatively intense during the period between the third and fourth sawtooth. Note that during the fourth injection, the tail current disrupts tailward of geostationary orbit, while the current around geosynchronous distance remains strong. It is also evident that throughout the period, the currents near and inside geosynchronous orbit are slowly increasing in intensity at the midnight meridian.

[46] The bottom panel reveals the strong asymmetry in the magnetospheric currents as well as the strong role of the

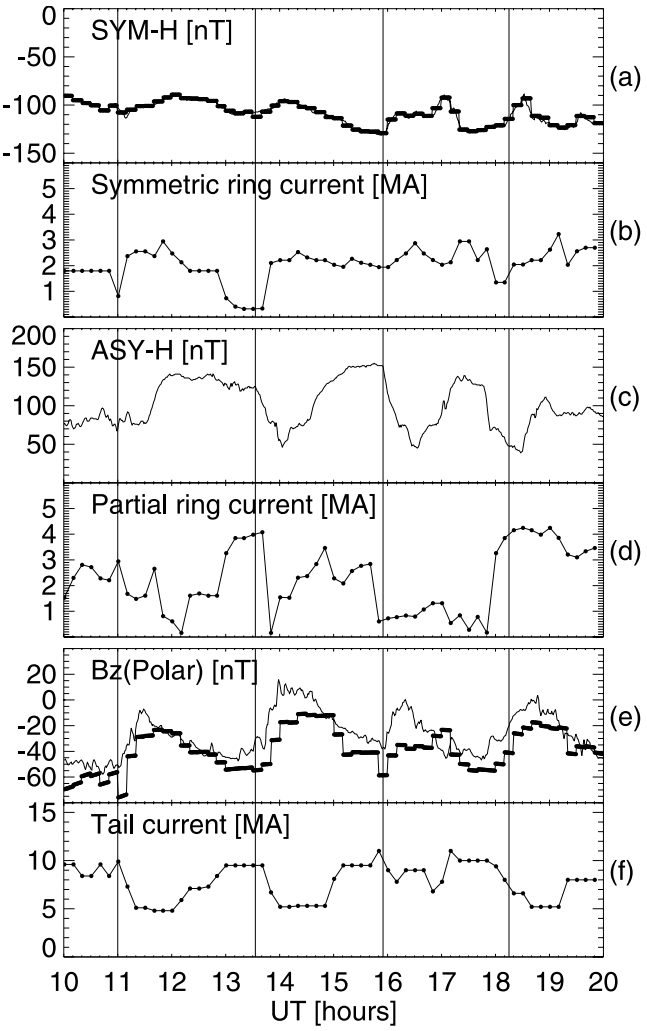

Figure 7. 2001-10-22: Model predictions of inner magnetosphere current systems. (a) SYM-H index (solid line) and model prediction (solid line with symbols); (b) Symmetric ring current intensity from the model; (c) ASY-H index; (d) Partial ring current intensity from the model; (e) B_Z from Polar (dipole field subtracted, thin solid line) and model prediction (solid line with symbols); (f) Tail current intensity from the model.

partial ring current in the dynamics of the event. The dusk sector (positive *Y*-values) currents are much stronger than those in the dawn sector, and also stronger than the tail currents in the near-Earth region. The three first sawteeth show a clear decrease of the partial ring current around the injection times (although for the first sawtooth the decrease is much delayed), but the fourth sawtooth shows a strong enhancement of the current, which remains at high level until the end of the modeling period.

[47] The top panel, showing the integrated currents inside geosynchronous orbit, reconfirm the model predictions shown in Figure 7: The dusk sector current (blue) has strong time variations and much resembles the partial ring current module in the model. In the other local time sectors, the time variability is much smaller and only show a gradual increase of the ring current throughout the period, again resembling the symmetric ring current module in the model. Thus it seems that the fitting procedure is able to distinguish the various current systems from the available observations quite well.

[48] The strong asymmetries in the magnetic field are clearly seen also in the field line configurations. Figure 9 shows the magnetic field lines at 1335 UT (shortly before the second sawtooth injection) for two meridional cuts, at the noon–midnight and dawn–dusk planes. The left panel showing the noon–midnight cut clearly illustrates the very strong currents that stretch the magnetotail to the degree that a neutral point is formed in the model. (As the model contains no plasma, formation of the neutral points occurs very easily, and auxiliary information should be used before these are interpreted as reconnection sites in the magnetotail). Furthermore, the right panel shows the effects of the highly asymmetric ring current with much-inflated dusk sector magnetic field configuration with stretched field lines.

[49] The middle panels of Figure 9 show the current intensity integrated in the *Z* direction (in units of nA/m) along the *X* (left) and *Y* (right) axes, depicting the total current through the noon-midnight and dawn-dusk meridian planes. The black curves give the currents at the time before the sawtooth injection (1335 UT), while the thin lines show the dipolarized field configuration after the injection at 1350 UT. The bottom panels show the same information, but integrated also along the radial direction from the Earth to the given radial distance. Thus, each point in the lower panels indicates the amount of current flowing inside that radial distance in the model. It is clear that before the sawtooth event, the current around geostationary orbit is very strong, being strongest in the dusk and midnight sectors. The effect of the injection is to move the current maximum closer to the Earth to provide the more dipolar field configuration, and the total current especially in the dusk sector decreases considerably. In the night sector, the total current inside 8 R_E does not actually change much: the effect is mostly a redistribution from the tail to the near-Earth region.

5. Discussion

[50] The sawtooth events discussed in this paper exhibit all typically found features: periodicity of about 2.5 hours, longitudinal range over 180 degrees within a relatively short time, and strongly asymmetric ring current. Thus conclusions drawn from this event are likely to hold for other sawtooth events as well.

5.1. Model Performance

[51] The event-oriented magnetic field model developed in this paper reproduced the magnetic field variations recorded at GOES 8, GOES 10, and Polar. These variations included strong field stretching prior to the sawtooth injections and dipolarizations of the field associated with the injections. The field inclination measurements not used in the model fitting were also reasonably well reproduced. These results lead us to believe that the empirical modeling techniques can be quite accurately used to reproduce the large-scale magnetospheric current systems during times

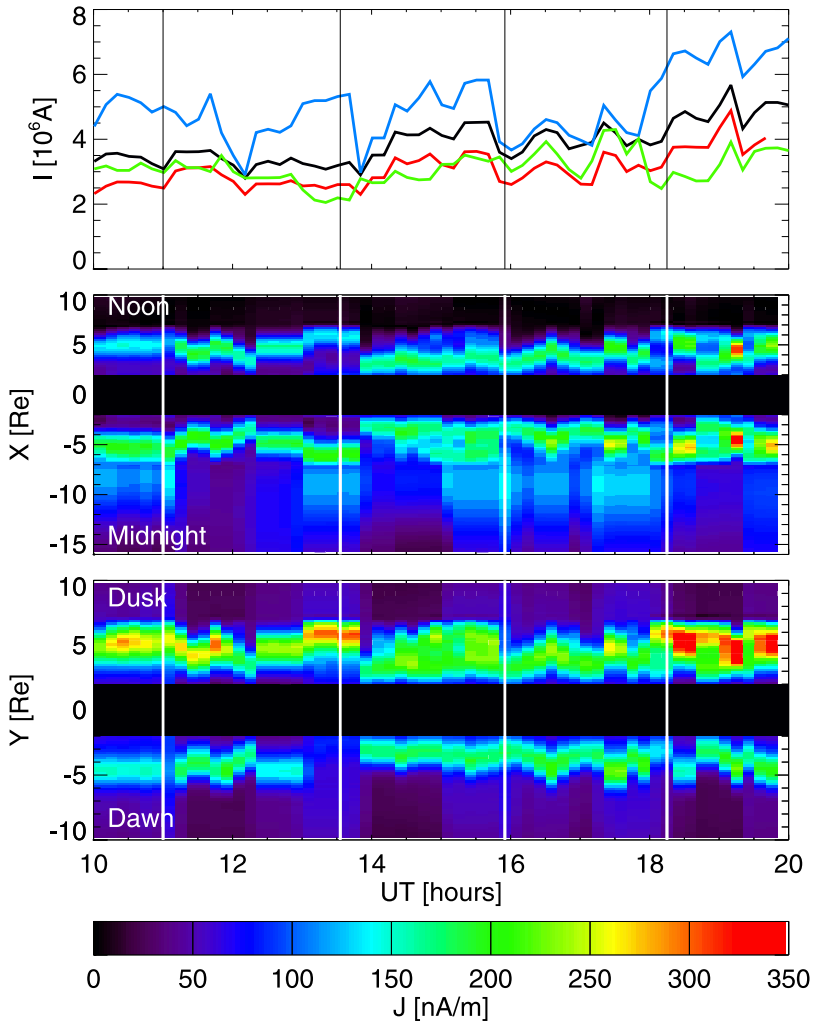

Figure 8. 2001-10-22: (top) Integrated current inside geostationary orbit (in units of MA) in four local time sectors, midnight (black), noon (red), dusk (blue), and dawn (green). (middle) Noon-midnight meridian cut of the current intensity integrated over the current sheet thickness. The current density is color-coded as function of time and *X*-distance along the tail. (bottom) Dawn-dusk meridian cut of the current intensity integrated over the current sheet thickness. The current density is color-coded as function of time and *Y*-distance along the terminator.

when observations from multiple locations in the inner magnetosphere are available.

[52] The model at times produces relatively fast variations of the symmetric ring current, which may not be consistent with the timescales of the ring current particle loss processes. However, it needs to be kept in mind that a magnetic field model responds both to variations in the ring current particle content (intensity of the current) and to changes in the field configuration (location of the current), which can lead to rapid changes in the field even if the particles remain in the inner magnetosphere. However, a future task might include examining a model version where the ring current is allowed to vary only slowly. This would have the largest effects on the current distribution between the partial ring current and the symmetric ring current, making the partial ring current even more variable than in the present version. As the model is already setting the largest variations to the partial ring current, the effects of this restriction may not be very large.

[53] The event-oriented magnetic field model provides current systems, their locations and intensities, and an optimal configuration to represent the data. While numerically tedious, the event-oriented approach gives a good representation of smaller-scale variations in the magnetic field, not provided by the statistical models, for problems which require detailed knowledge of the tail configuration and its changes over relatively short time periods. However, event-oriented modeling can only be applied to events where data are available from at least three well-positioned satellites covering the regions of interest in the magnetotail. Furthermore, the number of free parameters is large compared to the number of independent measurements in the magnetotail, and thus the determination of the model parameters requires careful analysis and parameter selection.

[54] Accurate representations of both magnetic and electric fields are needed for quantitative assessment of the effects of stormtime activations (be they substorms, sawtooth events, or other types of activations). Particle energi-

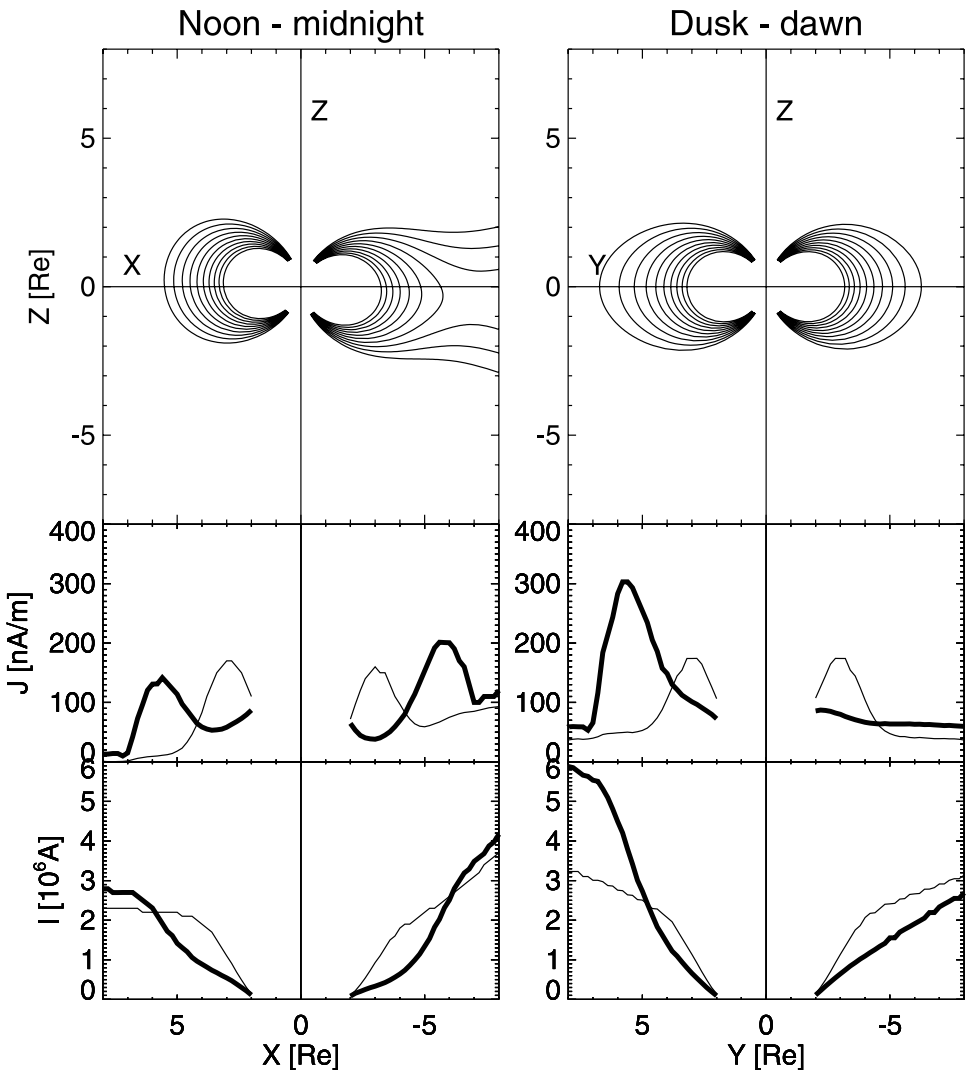

Figure 9. 2001-10-22: (top) Magnetic field lines at 1335 UT in the noon-midnight (left) and dawn-dusk (right) meridian planes. (middle) Current intensity (integrated in the vertical direction, in units of nA/m) as a function of X (left) and Y (right) for two time instants, before the second sawtooth injection at 1335 UT (thick line),and after the sawtooth injection at 1350 UT (thin line). (bottom) Integrated current (in units of A) as a function of X (left) and Y (right) in a format similar to the middle panel. The current values indicate total current inside that distance, thus the value at 6.6 R_E gives the current flowing inside geosynchronous orbit at that meridian.

zation and drift paths can be vastly different depending on the models used [*Ganushkina et al.*, 2006]. For example, using even strong but static convection electric field, it is impossible to reproduce the strong ion energization to 100-keV range. However, electric field impulses simulating the substorm effects together with more realistic magnetic field representations can account for the observed energy range and intensity of the ring current [*Ganushkina et al.*, 2005].

5.2. Sawtooth Events and Substorms

[55] The model results discussed above allow us to study the magnetospheric currents associated with the sawtooth events that demonstrated a wide local time extent of the stretching/dipolarization behavior. The magnetotail currents during sawtooth events resemble those during nonstorm substorms [e.g., *Pulkkinen et al.*, 1992]: A thin current sheet is formed in the inner magnetotail, and the sawtooth injections are associated with disruption of that current and consequent magnetic field dipolarization. The fact that the injections and field dipolarizations were seen almost simultaneously at geosynchronous orbit and at 8 R_E indicate that the sawtooth events are associated with large-scale magnetospheric processes that extend over several R_E in radial distance. These results are consistent with other event studies [*Henderson et al.*, 2006] and statistical properties of the sawtooth events.

[56] The differences between sawtooth events and substorms include a more Earthward intrusion of the tail current, which causes the inner edge of the current to close as a partial ring current [*Henderson*, 2004]. During sawtooth events, a strong, thin current sheet was present in the near-geostationary region encompassing not only the night-

side but also a significant portion of the dusk sector magnetosphere. This is a feature often found during magnetic storms, typical of the sawtooth events, but it is uncommon to find such tail-like fields in the dusk sector magnetosphere at other times [*Thomsen et al.*, 1994]. The empirical magnetic field model both reproduces the asymmetry and provides a qualitative explanation: an extension of a thin, tail current-like current carrying the partial ring current on open drift paths in the dusk sector.

[57] The strong partial ring current flows on open drift trajectories from the tail to the dusk sector. The extension of the current sheet toward the evening sector terminator significantly increases the drift speeds, and provides rapid access of the proton injections over a large portion of the geostationary orbit. *Henderson et al.* [2006] point out that the sawtooth injections are not necessarily simultaneous at all local times when examined in detail, and that the delays are consistent with propagation from the night sector toward dawn and dusk. Thus the current sheet extending close to the Earth and toward the dusk sector provides a qualitative explanation of the near-simultaneity of the injections at vastly different local times. On the other hand, the near-simultaneous field dipolarizations over a range of local times would suggest that the injection front was relatively wide.

[58] The SYM-H index increases (decrease in absolute value) slightly at each of the sawtooth onsets. While the symmetric ring current actually increases, the decrease of the partial ring current and tail currents dominate over the index to produce a net effect of increase. This once again highlights the fact that the SYM-H index (or the Dst index) responds to all magnetospheric current systems [*Turner et al.*, 2000]. Thus, careful analysis of all current systems is required before conclusions of the increase/decrease of the ring current can be drawn.

[59] While the dynamics of the sawtooth event onsets can be quite similar to nonstorm substorms (localized instability initiated within the thin current sheet formed in the inner magetotail [*Lui et al.*, 2004]), the consequences can be quite different: The strong convection drives the plasma sheet very close to the Earth and further duskward than under nonstorm conditions. This is clearly seen in the MPA data, which show that throughout the entire period, the geosynchronous spacecraft entered the plasma sheet between 1530 and 1700 MLT, which is 2–3 hours earlier in local time than under average conditions. The duskward extent of the tail current sheet causes a majority of the injected particles to be on open drift paths. This leads to the ring current's remaining relatively constant, while the asymmetry index undergoes strong variations. It is clear that such events will then have a different contribution to storm dynamics than those events, where the injected particles become mostly trapped on closed drift paths.

[60] The symmetric ring current (using Dst as a proxy) remained relatively constant during this period. *Pulkkinen et al.* [2005] analyzed the energy input and output using the Burton formulation [*O'Brien and McPherron*, 2000] and concluded that the constant driving from the solar wind was at a level where the losses were balanced by the driving, producing almost 24 hours of steady Dst. As neither the solar wind nor the IMF showed variations at the periodicity of the sawtooth injections, the cause of the 2.5-hour periodicity remains open.

[61] It is interesting to note that the empirical magnetic field model is able to reproduce the observed SYM-H variations to high degree of accuracy. Using the Dessler-Parker-Sckopke formulation based on ring current particle energy densities, *Siscoe et al.* [2005] recently showed results of the same storm obtained from the kinetic ring current RAM code by *Jordanova et al.* [1998]. The RAM code results were not able to reproduce the continued steady depression of the Dst, but predicted a faster decay of the index. *Siscoe et al.* [2005] argue that part of the discrepancy between the model and measured Dst arises from an overly large pressure correction; they argue that during strong activity the Chapman-Ferraro currents at the dayside magnetopause are changed to Region 1 currents connecting to the ionosphere. If this is the case, the correction due to those currents would be quite different from the one standardly applied (i.e., square root of the dynamic pressure), which was used here with good success. On the other hand, if the magnetic field configuration plays a major role in predicting the magnetic variations on ground, the dipole-based RAM code may be underestimating the current in the near-geostationary region.

[62] However, if indeed the magnetopause current topology is dependent on the intramagnetospheric currents, as recently suggested by *Palmroth et al.* [2006] and *Pulkkinen et al.* [2006], this further highlights the importance of having accurate information of the magnetospheric configuration when assessing questions related to solar wind and IMF drivers of magnetospheric activity.

6. Conclusions

[63] Analysis of a sawtooth event on 2001-10-22 using an empirical magnetic field model leads to the following conclusions:

[64] 1. Sawtooth injections are associated with strong stretching of both nightside and dusk sector magnetic field prior to the injection and a partial disruption of that current at the time of the injection. The currents are strongest near geosynchronous distance and in the premidnight sector.

[65] 2. The strong dusk-sector field stretching produces much faster proton drift times than in a quasi-dipolar field, which allows rapid expansion of the injection front. However, the near-simultaneous field dipolarization suggests a wide injection front. A wide injection front together with rapid drift times then provides the near-simultaneous configuration changes at all local times.

[66] 3. While the tail field behavior resembles that of nonstorm substorms, the consequences of the stretching/dipolarization cycle are different from nonstorm times: The drifting protons are mostly on open drift paths, which leads to lesser enhancement of the symmetric ring current and large variations in the asymmetric ring current.

[67] 4. Neither analysis of multipoint magnetic field data using the model nor analysis of the solar wind and IMF variations pointed to any explanation of the 2.5-hour recurrence time of the sawtooth events.

[68] 5. The three-spacecraft magnetic field measurements together with the Dst index were sufficient to constrain the model to give a reasonably accurate global magnetic field

representation, as confirmed by an independent test using the field inclinations from the geostationary spacecraft. This shows that the empirical modeling methods can be quite reliable in predicting the large-scale fields when suitable amount of observations are available.

[69] **Acknowledgments.** For the SuperMAG ground magnetometer data we gratefully acknowledge: The S-RAMP Database, PI K. Yumoto and K. Shiokawa; The SPIDR database; Intermagnet; The institutes who maintain the IMAGE magnetometer array; AARI data, PI Prof. Oleg Troshichev; Danish Meteorological Institute, Ole Rasmussen, and Project Scientist Jurgen Watermann; the CARISMA, PI Ian Mann; The MACCS program, PIs W. J. Hughes, and M. Engebretson as well as the Geomagnetism Unit of the Geological Survey of Canada; GIMA, PI John Olson; MEASURE, UCLA IGPP and Florida Institute of Technology; USGS, Jeffrey J. Love; MAGIC, PI. C. Robert Clauer; SAMBA, PI Eftyhia Zesta; 210 Chain, PI K. Yumoto; SAMNET, PI Farideh Honary; IMAGE, PI Ari Viljanen; the SuperMAG initiative, PI Jesper W. Gjerloev. TP thanks the IGPP for supporting her stay at the Los Alamos National Laboratory.

[70] Amitava Bhattacharjee thanks the reviewers for their assistance in evaluating this paper.

References

Bame, S. J., et al. (1993), Magnetospheric Plasma Analyzer for spacecraft with constrained resources, *Rev. Sci. Instrum.*, *64*, 1026.

Belian, R. D., G. R. Gisler, T. Cayton, and R. Christensen (1992), High-Z energetic particles at geostationary orbit during the Great Solar Proton Event series of October 1989, *J. Geophys. Res.*, *97*, 16,897.

Ganushkina, N. Y., T. I. Pulkkinen, M. V. Kubyshkina, H. J. Singer, and C. T. Russell (2002), Modeling the ring current magnetic field during storms, *J. Geophys. Res.*, *107*(A7), 1092, doi:10.1029/2001JA900101.

Ganushkina, N. Y., T. I. Pulkkinen, M. V. Kubyshkina, H. J. Singer, and C. T. Russell (2004), Long-term evolution of magnetospheric current systems during storm periods, *Ann. Geophys.*, *22*, 1317.

Ganushkina, N. Y., T. I. Pulkkinen, and T. Fritz (2005), Role of substorm-associated impulsive electric fields in the ring current development during storms, *Ann. Geophys.*, *23*(2), 579.

Ganushkina, N. Y., et al. (2006), Evolution of the proton ring current energy distribution during 21–25 April 2001 storm, *J. Geophys. Res.*, doi:10.1029/2006JA011609, in press.

Henderson, M. G. (2004), The May 2–3, 1986 CDAW-9C interval: A sawtooth event, *Geophys. Res. Lett.*, *31*, L11804, doi:10.1029/2004GL019941.

Henderson, M. G., G. D. Reeves, R. M. Skoug, M. F. Thomsen, M. H. Denton, S. B. Mende, T. J. Immel, P. C. Brandt, and H. J. Singer (2006), Magnetospheric and auroral activity during the 18 April 2002 sawtooth event, *J. Geophys. Res.*, *111*, A01S90, doi:10.1029/2005JA011111.

Huang, C.-S., G. D. Reeves, G. G. Le, and K. Yumoto (2005), Are sawtooth oscillations of energetic plasma particle fluxes caused by periodic substorms or driven by solar wind pressure enhancements?, *J. Geophys. Res.*, *110*, A07207, doi:10.1029/2005JA011018.

Iyemori, T., and D. R. K. Rao (1996), Decay of the Dst field of geomagnetic disturbance after substorm onset and its implication to storm-substorm relation, *Ann. Geophys.*, *14*, 608.

Jordanova, V. K., et al. (1998), October 1995 magnetic cloud and accompanying storm activity: Ring current evolution, *J. Geophys. Res.*, *103*, 79.

Kalegaev, V. V., N. Yu. Ganushkina, T. I. Pulkkinen, M. V. Kubyshkina, H. J. Singer, and C. T. Russell (2005), Relation between the ring current and the tail current during magnetic storms, *Ann. Geophys.*, *23*, 523.

Lui, A. T. Y., T. Hori, S. Ohtani, Y. Zhang, X. Y. Zhou, M. G. Henderson, T. Mukai, H. Hayakawa, and S. B. Mende (2004), Magnetotail behavior during storm time "sawtooth injections", *J. Geophys. Res.*, *109*, A10215, doi:10.1029/2004JA010543.

O'Brien, P., and R. L. McPherron (2000), An empirical phase space analysis of ring current dynamics: Solar wind control of injection and decay, *J. Geophys. Res.*, *105*, 7707.

Ogilvie, K. W., et al. (1995), SWE, A comprehensive plasma instrument for the Wind spacecraft, *Space Sci. Rev*, *71*, 55.

Palmroth, M., P. Janhunen, and T. I. Pulkkinen (2006), Hysteresis in the solar wind power input into the magnetosphere, *Geophys. Res. Lett.*, *33*, L03107, doi:10.1029/2005GL025188.

Pulkkinen, T. I., D. N. Baker, R. J. Pellinen, J. Büchner, H. E. J. Koskinen, R. E. Lopez, R. L. Dyson, and L. A. Frank (1992), Particle scattering and current sheet stability in the geomagnetic tail during the substorm growth phase, *J. Geophys. Res.*, *97*, 19,283.

Pulkkinen, T. I., N. Yu. Ganushkina, E. Donovan, X. Li, G. D. Reeves, C. T. Russell, H. J. Singer, and J. A. Slavin (2005), Storm-substorm coupling during 16 hours of Dst steadily at −150 nT, in *Inner Magnetosphere: Physics and Modeling*, *Geophys. Monogr. Ser.*, vol. 155, edited by T. I. Pulkkinen, N. A. Tsyganenko, and R. H. W. Friedel, p. 155, AGU, Washington, D. C.

Pulkkinen, T. I., M. Palmroth, E. I. Tanskanen, P. Janhunen, H. E. J. Koskinen, and T. V. Laitinen (2006), New interpretation of magnetospheric energy circulation, *Geophys. Res. Lett.*, *33*, L07101, doi:10.1029/2005GL025457.

Reeves, G. D., et al. (2004), IMAGE, POLAR, and geosynchronous observations of substorm and ring current ion injection, in *Disturbances in Geospace: The Storm-Substorm Relationship*, *Geophys. Monogr. Ser.*, vol. 142, edited by A. S. Sharma, Y. Kamide, and G. S. Lakhina, p. 91, AGU, Washington, D. C.

Russell, C. T., R. C. Snare, J. D. Means, D. Pierce, D. Dearborn, M. Larson, G. Barr, and G. Le (1995), The GGS Polar magnetic fields investigation, *Space Sci. Rev.*, *71*, 563.

Shue, J.-H., et al. (1998), Magnetopause location under extreme solar wind conditions, *J. Geophys. Res.*, *103*, 691.

Singer, H. J., L. Matheson, R. Grubb, A. Newman, and S. D. Bouwer (1996), Monitoring space weather with the GEOS magnetometers, *Proc. SPIE Int. Soc. Opt. Eng.*, *2812*, 299.

Siscoe, G. L., R. L. McPherron, and V. K. Jordanova (2005), Diminished contribution of ram pressure to Dst during magnetic storms, *J. Geophys. Res.*, *110*, A12227, doi:10.1029/2005JA011120.

Skoug, R. M., et al. (2003), Tail-dominated storm main phase: 31 March 2001, *J. Geophys. Res.*, *108*(A6), 1259, doi:10.1029/2002JA009705.

Smith, C. W., J. L. Heureux, N. F. Ness, M. H. Acuna, L. F. Burlaga, and J. Scheifele (1998), The ACE magnetic fields experiment, *Space Sci. Rev.*, *86*, 613.

Thomsen, M. F., S. J. Bame, D. J. McComas, M. B. Moldwin, and K. R. Moore (1994), The magnetospheric lobe at geosynchronous orbit, *J. Geophys. Res.*, *99*, 17,283.

Thomsen, M. F., D. J. McComas, G. D. Reeves, and L. A. Weiss (1996), An observational test of the Tsyganenko (T89a) model of the magnetospheric field, *J. Geophys. Res.*, *101*, 24,827.

Turner, N. E., D. N. Baker, T. I. Pulkkinen, and R. L. McPherron (2000), Evaluation of the tail current contribution to Dst, *J. Geophys. Res.*, *105*, 5431.

Tsyganenko, N. A. (1989), Magnetospheric magnetic field model with a warped tail current sheet, *Planet. Space Sci.*, *37*, 5.

Tsyganenko, N. A. (1995), Modeling the Earth's magnetospheric magnetic field confined within a realistic magnetopause, *J. Geophys. Res.*, *100*, 5599.

Tsyganenko, N. A. (2002a), A model of the near magnetosphere with a dawn-dusk asymmetry: 1. Mathematical structure, *J. Geophys. Res.*, *107*(A8), 1179, doi:10.1029/2001JA000219.

Tsyganenko, N. A. (2002b), A model of the near magnetosphere with a dawn-dusk asymmetry: 2. Parameterization and fitting to observations, *J. Geophys. Res.*, *107*(A8), 1176, doi:10.1029/2001JA000220.

N. Y. Ganushkina and E. I. Tanskanen, Finnish Meteorological Institute, P. O. Box 503, FIN-00101 Helsinki, Finland. (eija.tanskanen@fmi.fi; nataly.ganushkina@fmi.fi)

J. Gjerloev, Johns Hopkins University Applied Physics Laboratory, 11100 Johns Hopkins Rd, Laurel, MD 20723-6099, USA. (jesper.gjerloev@jhuapl.edu)

M. Kubyshkina, Institute of Physics, University of St. Petersburg, Petrodvoretz, St. Petersburg 198504, Russia. (kubysh@geo.phys.spbu.ru)

T. I. Pulkkinen, G. D. Reeves, and M. F. Thomsen, Los Alamos National Laboratory, ISR-1, MS 466, Los Alamos, NM 87545, USA. (tuija@lanl.gov; reeves@lanl.gov; mthomsen@lanl.gov)

C. T. Russell, Institute of Geophysics and Planetary Physics, University of California, Los Angeles, Los Angeles, CA 90024-1567, USA. (ctrussel@igpp.ucla.edu)

H. J. Singer, NOAA Space Environment Center, 325 Broadway, Boulder, CO 80305, USA. (howard.singer@noaa.gov)

J. A. Slavin, NASA Goddard Space Flight Center, Code 696, Greenbelt, MD 20771, USA. (james.a.slavin@nasa.gov)